JOURNAL OF THERMOPHYSICS AND HEAT TRANSFER
Vol. 23, No. 1, January–March 2009

Solution of the Nonlinear Heat Equation for Circular-Foil Heat Flux Gauges

Anthony M. Agnone*
Hofstra University, Hempstead, New York 11549

DOI: 10.2514/1.34206

A series solution of the steady nonlinear heat equation for a circular-thin-foil heat flux gauge subjected to a constant-radiation heat flux is presented. The dimensionless form of the heat equation involves a dimensionless gauge parameter and a dimensionless irradiation parameter. A linear solution is extracted from the series solution, which yields a simple-yet-accurate formula that is useful for calibration of thin-foil heat flux gauges. The dimensionless temperature at the center of the foil is determined from the linear solution as a function of the preceding two parameters. The dependence of the irradiation parameter on the dimensionless temperature at the center of the circular foil is presented graphically for a wide range of the parameters. The values of the dimensionless temperature at the center of the foil obtained with the linear solution are in good agreement with those obtained with a numerical solution of the heat equation using Runge–Kutta integration. Typical temperature profiles also show good agreement with the numerical solution. To compensate for inherent gauge errors and assumptions made in the analysis, individual gauges are calibrated against standards. To curve fit the calibration data, it is suggested that a correction factor be introduced in the argument of the modified Bessel function that appears in the linear formula for the dimensionless irradiation parameter.

Nomenclature

A	=	dimensionless gauge parameter ($\varepsilon\sigma R^2 T_R^3/kt$)
a_n	=	coefficients in the series solution of the dimensionless temperature, Eq. (7)
B	=	dimensionless irradiation parameter ($H/\sigma T_R^4$)
BL	=	dimensionless irradiation parameter obtained with the linear solution (B_L), Eq. (12)
C	=	constants in the series solution of the dimensionless temperature, Eqs. (7a–7g)
F	=	function for determining the values of θ_o
H	=	irradiation, W/m^2
Io	=	modified Bessel function of order zero
k	=	thermal conductivity of the foil, W/m K
R	=	radius of the foil, m
r	=	radial coordinate, m
T	=	temperature, K
TR	=	temperature of the copper heat sink (T_R), K
T_R	=	temperature of the copper heat sink, K
t	=	foil thickness, m
$\Delta\theta$	=	dimensionless temperature difference [$\theta(0) - 1$]
ε	=	emittance
η	=	dimensionless radius squared (ρ^2)
θ	=	dimensionless temperature (T/T_R)
θo	=	dimensionless temperature at the center of the foil (θ_o)
ξ	=	transformed independent variable [$(AB^{3/4}/4)\rho^2$]
ρ	=	dimensionless radial coordinate (r/R)
σ	=	Stefan–Boltzmann constant (5.67×10^{-8}), W/m^2 K^4
ϕ	=	transformed dependent variable [$\theta(\eta)/B^{1/4}$]

Subscripts

i, n	=	indices used in the series solution of the dimensionless temperature, Eq. (7f)
L	=	linear solution
o	=	value at the center of the foil ($r = \rho = \eta = 0$)
R	=	edge of the foil where $r = R$
s	=	denotes series solution

Received 22 August 2007; revision received 22 September 2008; accepted for publication 17 October 2008.

*Professor Emeritus, Department of Engineering, 211 Weed Hall. Associate Fellow AIAA.

I. Introduction

HEAT flux measurements are routinely performed in industrial processes, fire research, aerospace, and photography. In industrial processes, control of the heating process is necessary to avoid too rapid heating or exceeding a maximum allowable temperature. In aerospace applications, heat flux measurements are needed to design the thermal protection systems of devices such as rocket nozzles, combustors, and leading edges or windward surfaces of hypersonic vehicles. Heat flux gauges are also used in ground-test facilities, such as high-speed wind tunnels, to detect laminar-to-turbulent boundary-layer transition, for example. In addition to temperature measurements, heat flux rates are needed to assess the performance of devices that operate at elevated temperatures. A succinct summary of the need for heat flux measurements in scientific and industrial endeavors as well as the usage and construction of a typical heat flux gauge is provided in [1].

Many heat flux designs have been developed to suit specific applications [2]. Gauges are typically classified as a diffusion type or one-dimensional plug (calorimeter) type. A cross section of a diffusion-type heat flux gauge, commonly called a Gardon gauge, is shown in Fig. 1. The foil is mounted at the circumference on an oxygen-free high-conductivity copper heat sink that is maintained at a constant temperature T_R. A recent patent that describes a construction method of a heat flux gauge in great detail may be found in [3]. Before use, a particular gauge design is calibrated against standards to correct for inherent errors and to determine their limitations [4,5]. Some gauges are used to measure total heat flux, whereas others are designed to measure only the radiation part of the total heat flux. In the latter designs, a thermally isolated thin layer of sapphire is placed over the sensing element to avoid measuring the convective heat transfer component. The sensing surface of the thin foil is also coated with suitable black substances to insure a high-absorptivity coefficient. A temperature difference on the foil is made in conjunction with a theoretical heat transfer analysis to relate the temperature difference to the heat flux incident on the foil in a linear relation [6,7]. However, when the thin foil is subjected to radiation

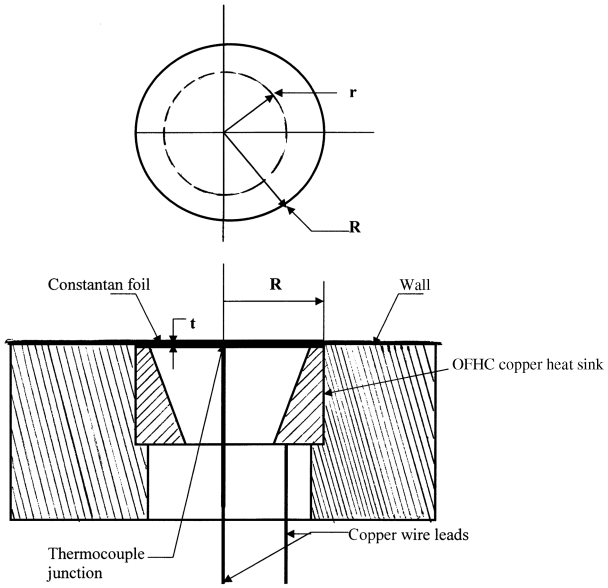

Fig. 1 Typical cross section of a thin-foil heat flux gauge (OFHC denotes oxygen-free, high-conductivity).

heat transfer, the relation becomes nonlinearly dependent on the temperature difference.

II. Analysis and Results

To determine the nonlinear relation, a steady-state thermophysical model of a thin, circular, constantan-foil heat flux gauge, shown schematically in Fig. 1, that is subjected to a constant irradiation flux H is presented in [1]. The restrictions and requirements for the applicability of the mathematical model are also expounded there. The gauge is presumed to be in a vacuum so that there is negligible heat transfer to or from the lower surface of the foil. The foil is thin so that its temperature is uniform normal to the foil and there is heat conduction in the radial direction only. The governing heat equation for the foil temperature is subjected to two boundary conditions: 1) a constant temperature T_R at $r = R$ and 2) a symmetry condition at the center (i.e., $dT/dr = 0$ at $r = 0$). The heat equation and boundary conditions for the dimensionless foil temperature $\theta(\rho)$, where $\rho = r/R$, are found in [1] as Eqs. 4–6, which, in terms of the dimensionless variables θ and ρ, are given as

$$\frac{1}{\rho}\frac{d}{d\rho}\left(\rho\frac{d\theta}{d\rho}\right) = A\theta^4 - AB \tag{1}$$

$$\left(\frac{d\theta}{d\rho}\right)\bigg|_{\rho=0} = 0 \tag{2}$$

$$\theta(1) = 1 \tag{3}$$

where A is a dimensionless gauge parameter defined in [1] as

$$A = \frac{\varepsilon\sigma R^2 T_R^3}{kt} \tag{4}$$

The parameter A is a dimensionless grouping of the foil dimensions and its thermophysical and radiative properties. When the numerator and denominator of Eq. (4) are multiplied by T_R, Eq. (4) expresses the relative importance of heat transfer by radiation from the foil to that by heat conduction. Hence, when A is small (say, 0.01 or less), heat conduction in the foil is dominant. Radiative heat transfer is dominant when the product AB is greater than order 1. B is a dimensionless irradiation parameter defined as

$$B = \frac{H}{\sigma T_R^4} \tag{5}$$

It is a similarity parameter that expresses the relative importance of the irradiation flux onto the foil to a measure of the heat flux by radiation from the foil. The similarity parameters A and B are useful for scaling heat flux data obtained with similar gauge designs.

Equation (1) is solved in [1] using a Green's function approach and the method of successive approximations. For each value of A, the parameter B is calculated as a function of the dimensionless temperature difference (i.e., $\Delta\theta = \theta_o - 1$, where θ_o is the dimensionless temperature at the center of the foil). The nonlinear nature of the functional dependence of B on A and $\Delta\theta$ was then curve-fitted. The authors of [1] recommend adjusting the geometric parameters of the gauge (i.e., its radius R) and the thickness of the foil t and surface emissivity to have the gauge parameter A fall between 0.1 and 100 so as to minimize the influence of the presence of the gauge on the wall temperature of the test article on which the gauge is mounted.

Here, Eq. (1) is solved by noting the solution is an even function of ρ. Accordingly, Eq. (1) is transformed by letting $\eta = \rho^2$. Then the transformed equation is solved by obtaining a finite series expansion for ρ up to the 10th power. It is found that the series solution embodies the solution of the linear form of Eq. (1). The purpose of this article is to provide an algebraic relation for the dependence of B on A and $\Delta\theta$. Accordingly, an assessment of the accuracy of the linear solution is presented by comparing the dimensionless temperature profiles and the dependence of B on A and $\Delta\theta$ with a numerical solution of Eq. (1), which was performed using Runge–Kutta (R-K) integration. The present solution offers physical insight and provides a simple analytic expression that can be used for calibration, design, and optimization of heat flux gauges.

A. Preliminary Observations

Before the presentation of the numerical solution, some observations are stated next. Equation (1) admits a general solution $\theta(\rho) = \text{constant} = \pm B^{1/4}, \pm iB^{1/4}$, where $i = \sqrt{-1}$. Only the case $B = 1$ satisfies the boundary conditions. When the thermal conductivity is zero and A is correspondingly infinite, the solution is such that the dimensionless temperature at the center, $\theta(0) = \theta_o$, is equal to $B^{1/4}$. For $A = 0$ or $B = 1$, the solution is $\theta(\eta) = 1$ for all values of B or A, respectively. For $0 \le B < 1$, the foil temperature is less than T_R everywhere on the foil, due to radiation cooling from the foil, so that $\theta(\eta) \le 1$. A solution of the preceding problem exists if and only if θ_o is less than or equal to $B^{1/4}$.

The parameters A and B that occur in Eq. (1) can be readily absorbed by using the following two transformed variables: $\xi = (AB^{3/4}/4)\rho^2$ and $\phi(\xi) = \theta(\rho)/B^{1/4}$. The transformed form of Eq. (1) is void of the parameters A and B. The first transformed variable shows that the solution is an even function of ρ. Unfortunately, the boundary conditions become dependent on A and B so that no universal solution can exist. These transformations indicate that the dimensionless temperature θ scales with $B^{1/4}$, and ρ scales with the square root of the product $AB^{3/4}$. Equation (1) shows that θ depends on the parameter A and the product AB. The product AB is also a dimensionless similarity parameter that expresses the relative importance of irradiation and heat conduction. However, because the dependence of B on A and $\Delta\theta$ is being sought here, the solution of Eq. (1) is performed for pair of values of A and B.

B. Numerical Solution Using Runge–Kutta Integration

Equations (1–3) constitute a standard split-boundary-value problem that requires shooting techniques in which the unknown initial condition (θ_o here) is iterated until the edge condition, Eq. (3), is satisfied. Several numerical integration schemes, finite difference methods, and least-squares fit techniques have been developed to solve similar nonlinear equations [8]. Advanced methods require, in addition to the differential equation, the introduction of an auxiliary differential equation that is used for determining the unknown initial

condition [8,9]. A Newton root-locating technique is used to iterate on the initial condition.

Here, the numerical solution of Eq. (1) was performed using a R-K algorithm [8] as an initial-value problem by prescribing an initial value of θ_o and then iterating on it. The linear solution was used to provide the initial iterate of θ_o. This reduced the computation effort and it also provided a check on the accuracy of the value of θ_o obtained from the linear solution. A small step size, $\Delta\rho = 0.0001$, was used in most of the cases presented here. However, for values of A and B, such that $AB^{3/4}$ was greater than about 10, large thermal gradients occurred close to the edge of the foil. In these cases, the step size was reduced to 10^{-6} and the value of θ_o had to be iterated to many significant figures to satisfy the edge condition $\theta(1) = 1$ to at least five significant figures. For example, for $A = 1$ and $B = 200$, a step size $\Delta\rho = 10^{-6}$ was used and the value of the dimensionless temperature θ_o at the center of the foil was iterated to 3.7605845556917 to satisfy the edge boundary condition, Eq. (3), to an error of 1.072×10^{-8}. This value of θ_o is 0.000493% less than the asymptotic value, which is $200^{1/4} = 3.760603093\ldots$. In addition to the step size, the accuracy of the numerical integration using R-K was controlled by setting the error tolerance in the R-K algorithm for convergence at 10^{-8}.

The individually calculated values of the dimensionless temperature at the center of the foil θ_o obtained using R-K integration are listed rounded-off to five significant figures in Table 1 for A ranging from 0.0 to 100. The values of θ_o listed in the first row of Table 1 correspond to $B = 0$, which occurs when the irradiation to the foil is zero. As stated in the section under Preliminary Observations, for $B = 1$, which corresponds to $H = 459.3$ W/m^2 when $T_R = 300$ K, the values of θ_o are unity for all values of A. The last column in Table 1 lists the asymptotic values of θ_o when A is infinite (i.e., $B^{1/4}$). The asymptotic values of θ_o are listed to seven significant figures without round-off. The values of θ_o listed in the bottom row of Table 1 in the columns under $A = 10$ and 100 are listed the same as the asymptotic values but rounded to five significant figures.

C. Series Solution

A series solution was obtained by noting that Eq. (1) and the boundary conditions indicate that the solution is a function of powers of ρ^2. The physical reason for this is that the temperature is uniformly distributed over circular discs for which the areas are proportional to the square of the radius. Therefore, letting $\eta = \rho^2$, Eq. (1) transforms into

$$\eta\frac{d^2\theta}{d\eta^2} + \frac{d\theta}{d\eta} = \frac{A}{4}(\theta^4 - B) \tag{6}$$

A Maclaurin series solution of Eq. (6) was developed by evaluating the derivatives of θ, with respect to η, at $\eta = 0$. That is, assuming

$$\theta_S(\eta) = \theta_o + \sum_{n=1}^{\infty}\frac{a_n}{n!}\eta^n \tag{7a}$$

where θ_o is the dimensionless temperature at the center of the foil, $\eta = 0$. The first derivative a_1 is obtained directly from Eq. (6) as

$$a_1 = \left.\frac{d\theta}{d\eta}\right|_{\eta=0} = \frac{A}{4}(\theta_o^4 - B) \tag{7b}$$

The second and higher derivatives with respect to η [i.e., $a_n = (d^n\theta/d\eta^n)|_{\eta=0}$] are obtained by repeated differentiation of Eq. (6) and evaluation at $\eta = 0$. The second through fifth derivatives are

$$a_2 = \left(\frac{A\theta_o^3}{2!}\right)a_1 \tag{7c}$$

$$a_3 = \left(\frac{(A\theta_o^3)^2}{3!}\right)a_1 + A\theta_o^2 a_1^2 \tag{7d}$$

$$a_4 = \left(\frac{(A\theta_o^3)^3}{4!}\right)a_1 + \frac{11}{8}A^2\theta_o^5 a_1^2 + \frac{3}{2}A\theta_o a_1^3 \tag{7e}$$

$$a_5 = \left(\frac{(A\theta_o^3)^4}{5!}\right)a_1 + \frac{9}{8}A^3\theta_o^8 a_1^2 + \frac{63}{10}A^2\theta_o^4 a_1^3 + \frac{6}{5}Aa_1^4 \tag{7f}$$

After substituting a_1 into Eqs. (7b–7e), a_n are of the form

$$a_n = A^n\sum_{i=2}^{n} C_{i,n}\theta_o^{3n-4i+5}(\theta_o^4 - B)^{i-1} \tag{7g}$$

where $C_{i,n}$ are the rational numbers appearing in Eqs. (7b–7e). The series solution can be extended by further differentiation of Eq. (6). However, this becomes tedious and cumbersome. Also, the series solution does not yield an explicit relation for dimensionless irradiation parameter B.

The dimensionless temperature at $\eta = 0$ is found by imposing the edge boundary condition, Eq. (3), to get

$$F(\theta_o, A, B) = 1 - \theta_o - \sum_{n=1}^{\infty}\frac{a_n}{n!} = 0 \tag{8}$$

The function $F(\theta_o, A, B) = 0$, using Eq. (8) with six terms, is plotted in Fig. 2 for $A = 1$ and three values of B. Figure 2 shows the migration of a negative root of Eq. (8) to the positive side of the abscissa as B increases from 17 to 25. The negative roots of F imply negative temperatures and hence are not physically realistic. When B is less than about 19.8, only one real positive root occurs. As B increases above 19.8, multiple positive real roots occur. Only the largest root results in physically meaningful temperature profiles. The smaller positive roots produce profiles that exhibit negative temperatures. Similarly, for $A = 0.5$ and 10, multiple roots occur when B is about 49 and 0.98, respectively. A study of the function $F(\theta_o, A, B) = 0$ shows that for given values of A and B, multiple positive values of θ_o can occur when $AB^{3/4}$ is greater than about 10. Specifically, if only the first term in the summation in Eq. (8) is considered, then θ_o appears in a_1 to the fourth power. Hence, in

Table 1 Values of dimensionless temperature at the center of the foil θ_o from Runge–Kutta integration

	A							
B	0	0.001	0.01	0.10	1.0	10	100	∞
0	1	0.99975	0.99757	0.97671	0.84743	0.55665	0.29591	0.0000000
0.001	1	0.99975	0.99752	0.97670	0.84890	0.55755	0.30208	0.1778279
0.01	1	0.99975	0.99754	0.97694	0.85024	0.56560	0.34978	0.3162277
0.1	1	0.99977	0.99776	0.97904	0.86384	0.64843	0.56281	0.5623413
1	1	1	1	1	1	1	1	1
10	1	1.00225	1.02232	1.20513	1.72966	1.77827	1.77827	1.7782794
100	1	1.02473	1.24503	2.68367	3.16193	3.16219	3.16227	3.1622776
1000	1	1.24949	3.32816	5.61136	5.62280	5.62341	5.62341	5.6234132

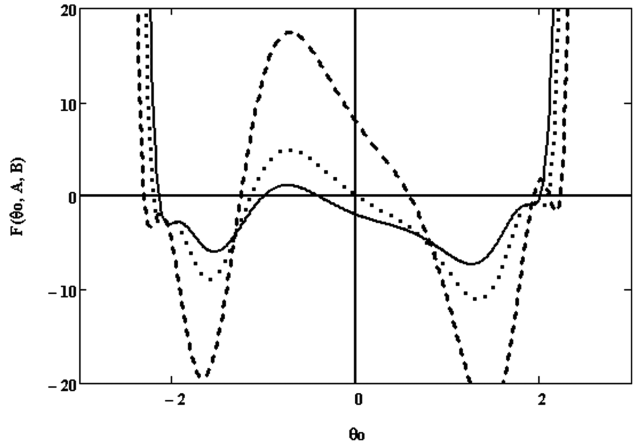

Fig. 2 Function $F(\theta_o, A, B)$ for finding values of dimensionless temperature θ_o at the center of the foil for $A = 1$ (solid curve: $B = 17$; dotted curve: $B = 19.8$; and dashed curve: $B = 25$).

general, there could be four roots. Inclusion of additional terms in the series gives rise to additional roots according to the largest exponent of θ_o in the truncated series. Numerical experimentation shows that the truncated series solution represented by Eqs. (7a–7f) converges for $A \leq 1$ and $B \leq 100$. The values of θ_o, obtained using the series solution, Eq. (8), are compared graphically in Fig. 3 with those obtained using the R-K algorithm. The values of θ_o, determined using the Runge–Kutta integration, appear as geometric symbols in Fig. 3. Within the range of convergence of the series solution, the difference between the values of θ_o obtained from the series solution, Eq. (8), and those obtained by numerical integration of Eq. (1) using R-K are less than 1%.

By combining Eqs. (7a) and (8), the series solution can also be written as

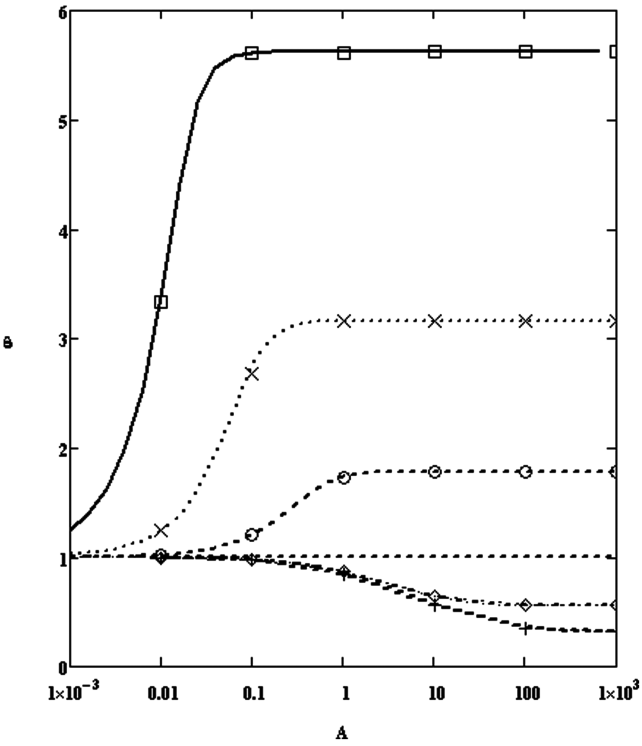

Fig. 3 Plot of θ_o as a function of A for several values of B [curves: linear solution, Eq. (11); geometric symbols: points calculated by numerical integration of Eq. (1) using a Runge–Kutta algorithm; solid curve and squares: $B = 1000$; dotted curve and X-X-X: $B = 100$; dashed curve and circles: $B = 10$; dash-dot curve and diamonds: $B = 0.1$; and dark dash and + + +: $B = 0$].

$$\theta_S(\eta) = 1 + \sum_{n=1}^{\infty} \frac{a_n}{n!}(\eta^n - 1) \tag{9}$$

Note that Eq. (9) is not a Taylor series expansion for $\theta_s(\eta)$ about $\eta = 1$. In this form the unknown θ_o is not isolated as in Eq. (7a).

D. Linear Solution

The series solution does not yield an explicit relation for B as a function of A and $\Delta\theta$. Considerable computational effort is required to obtain the value of θ_o for each pair of values of A and B and to obtain the functional dependence of B on A and $\Delta\theta$ for a wide range (six decades) of A. In the end, the functional dependence computed using the series solution must be expressed graphically or curve-fitted as was done in [1]. Here, an algebraic expression for the dimensionless irradiation parameter B is being sought that could be suitable for gauge design and calibration purposes at minimum expense to accuracy. Fortunately, such an expression for the dimensionless irradiation parameter was found by collecting the linear terms in a_1 in the series solution. Retaining only the linear terms in a_1, in a_n, the series solution can be simplified by noting that the summation is related to the series expansion for the modified Bessel function of order 0 ([10], Eq. 9.6.12). The linear form of the series expansion becomes

$$\theta_L(\eta) = \theta_o - \left(\frac{B - \theta_o^4}{4\theta_o^3}\right)\left[Io\left(\sqrt{4\theta_o^3 A\eta}\right) - 1\right] \tag{10}$$

where the subscript L denotes the linear solution. Note that the edge condition, Eq. (3), has not been satisfied yet. The linear solution, Eq. (10), neglects the quadratic and higher-power terms containing a_1 in the series solution, Eq. (7), which become negligible as θ_o approaches the asymptotic value $B^{1/4}$. The first contribution of the quadratic terms in a_1 appears in the second term of the coefficient a_3, Eq. (7d), which is multiplied in the series solution, Eq. (7a), by $\eta^3/3! = \rho^6/6 \leq 0.167$ because $\eta \leq 1$. Hence, the linear solution is accurate for r to about the fifth power and therefore it should yield good results. The value of θ_o consistent with the linear solution is obtained by imposing the edge condition, Eq. (3), at $\eta = 1$. That is,

$$\theta_L(1) = 1 = \theta_o - \left(\frac{B - \theta_o^4}{4\theta_o^3}\right)\left[Io\left(\sqrt{4\theta_o^3 A}\right) - 1\right] \tag{11}$$

The values of θ_o obtained from Eq. (11) are listed in Table 2 for A and B ranging from 0 to 100. Unlike the series solution, Eq. (11) yields only one positive root. The last column in Table 2 lists the asymptotic values as in Table 1. A comparison of the values of θ_o listed in Table 2 with those listed in Table 1 shows a maximum error of 6.1% when B is greater than one. This error occurs when θ_o falls in the rapid rise portion of the curves shown in Fig. 3. The accuracy of the linear solution is addressed further in the next section. The dimensionless parameter B is obtained from Eq. (11) as

$$B_L = \theta_o^4 + \left(\frac{4\theta_o^3(\theta_o - 1)}{Io(\sqrt{4\theta_o^3 A}) - 1}\right) \tag{12}$$

Equation (12) is the relation that is being sought here. It is an explicit relation for B_L and is exact:

1) When θ_o equals one, yielding $B_L = 1$ for all values of A.

2) As A approaches infinity, $B_L = \theta_o^4$.

3) For $A = 0$, $\theta_o = 1$ for all values of B!

A graphical presentation of B_L and comparison with the values obtained using R-K is shown in Fig. 4 as a function of $\Delta\theta$ for four values of A. Figure 4 corresponds to Fig. 5 of [1]. The numerical accuracy of Eq. (12) is addressed in the section on accuracy of the linear solution.

The linear solution, Eq. (10), for the dimensionless temperature profiles can be expressed in two alternate forms. Equation (11) is solved for the $(B - \theta_o^4)/(4\theta_o^3)$ term, which is then substituted into Eq. (10) to get the first equality:

Table 2 Values of dimensionless temperature at the center of the foil θ_o from Eq. (11)

	A							
B	0	0.001	0.01	0.10	1.0	10	100	∞
0	1.0	0.99975	0.99752	0.97675	0.84928	0.57318	0.32827	0.0000000
0.001	1.0	0.99975	0.99752	0.97666	0.84911	0.57385	0.33242	0.1778279
0.01	1.0	0.99975	0.99754	0.97687	0.85057	0.58093	0.36666	0.3162277
0.1	1.0	0.99978	0.99776	0.97898	0.86505	0.64632	0.56310	0.5623413
1	1.0	1.00000	1.00000	1.00000	1.00000	1.00000	1.00000	1.0000000
10	1.0	1.00225	1.02232	1.20575	1.73821	1.77818	1.77816	1.7782794
100	1.0	1.02381	1.24432	2.75649	3.16202	3.16213	3.16210	3.1622776
1000	1.0	1.24926	3.39039	5.61579	5.62340	5.62325	5.62322	5.6234132

$$\theta_L(\eta) = \theta_o - (\theta_o - 1)\left[\frac{Io(\sqrt{4\theta_o^3 A\eta}) - 1}{Io(\sqrt{4\theta_o^3 A}) - 1}\right]$$
$$= \left(\frac{B + 3\theta_o^4}{4\theta_o^3}\right) - \left(\frac{B + 3\theta_o^4}{4\theta_o^3} - 1\right)\left[\frac{Io(\sqrt{4\theta_o^3 A\eta})}{Io(\sqrt{4\theta_o^3 A})}\right] \quad (13)$$

The second equality is obtained by first adding the θ_o to $(B - \theta_o^4)/(4\theta_o^3)$ in Eq. (10) to get $(B + 3\theta_o^4)/4\theta_o^3$. The ensuing equation is evaluated at $\eta = 1$ and is solved for the $(B - \theta_o^4)/(4\theta_o^3)$ term, which is now the multiplying factor for only the modified Bessel function term. Then the equality of that term is substituted into Eq. (10) to yield the second equality shown in Eq. (13). The reason for writing Eq. (13) in the second form will become apparent next.

The product $4\theta_o^3$ in the series expansion and in the argument of the modified Bessel function is the slope of the quartic θ^4 evaluated at $\eta = 0$, where $\theta = \theta_o$. That is, as shown in Fig. 5, a linearization of the quartic can be achieved by taking the following linear form for the quartic near $\theta = \theta_o$:

$$\theta^4 \cong 4\theta_o^3\theta - 3\theta_o^4 \quad (14)$$

As shown in Fig. 5, a least-squares fit line of the quartic between $\theta = 1$ and θ_o can also be used. A secant of the quartic is also shown in Fig. 5 for reference. Although the least-squares fit line minimizes the error by the linear representation of the quartic, it results in cumbersome expressions. Therefore, it is not presented here. Although Eq. (14) is valid close to the center, it yields negative values for θ^4 when θ is less than $3/4\theta_o$. Nevertheless, the solution of the linear form of Eq. (1) obtained using Eq. (14) also results in the second equality shown in Eq. (13), which corresponds to Eq. 10 of [1], with A replaced by $4\theta_o^3 A$ and B replaced with $(B + 3\theta_o^4)/(4\theta_o^3)$.

The dimensionless temperature profiles $\theta(\rho)$ using either form of Eq. (13) with η replaced by ρ^2 and θ_o obtained from a solution of Eq. (11) are compared in Figs. 6a–6c with profiles obtained by numerical integration using R-K for the same three cases reported in Fig. 2 of [1]. For these three cases, the maximum difference in the dimensionless temperature profiles occurs at the center, $\rho = 0$. The percent errors between the linear solution and the R-K solution at the center are 0.057, 0.49, and 0.14% for the values of A and B reported in Figs. 6a–6c, respectively. The temperature profiles obtained with Eq. (13) are in good agreement with those obtained by numerical integration of Eq. (1) using R-K. For $B \ll 1$, the temperature at the center of the gauge is less than at the edge (i.e., $T_o < T_R$). This implies the following:

1) The radiative heat emitted by the foil is greater than that received by irradiation.

2) There is heat conduction from the heat sink *into* the foil of the gauge.

An additional profile for $A = 10$ and $B = 10$ is presented in Fig. 6d. This shows a large thermal gradient close to the edge. The error at the center is 0.0056%. A maximum error of 3.25% between

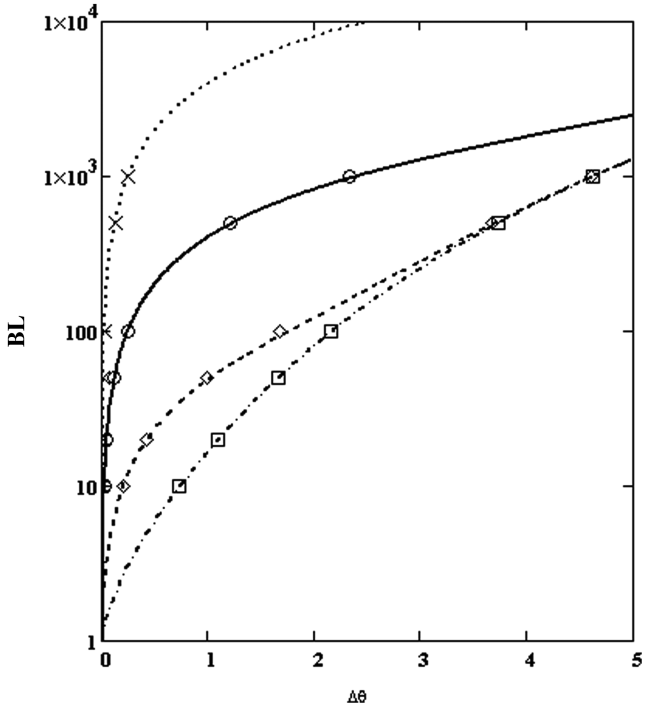

Fig. 4 Plot of dimensionless irradiation parameter B_L as a function of the dimensionless temperature difference $\Delta\theta$ from Eq. (12) and comparison with Runge–Kutta integration (geometric symbols) (dotted curve and X-X-X: $A = 0.001$; solid curve and circles: $A = 0.01$; dashed curve and diamonds: $A = 0.1$; and dash-dot curve and squares: $A = 1$).

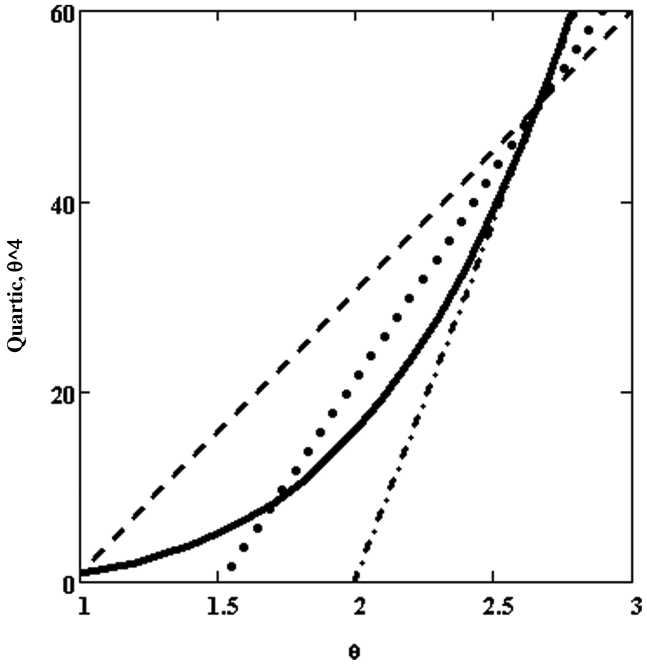

Fig. 5 Linear representation of quartic θ^4 using tangent, least-squares fit, and secant [solid curve: quartic θ^4; dashed curve: secant; dotted curve: least-squares fit; and dash-dot curve: tangent at (θ_o, θ_o^4)].

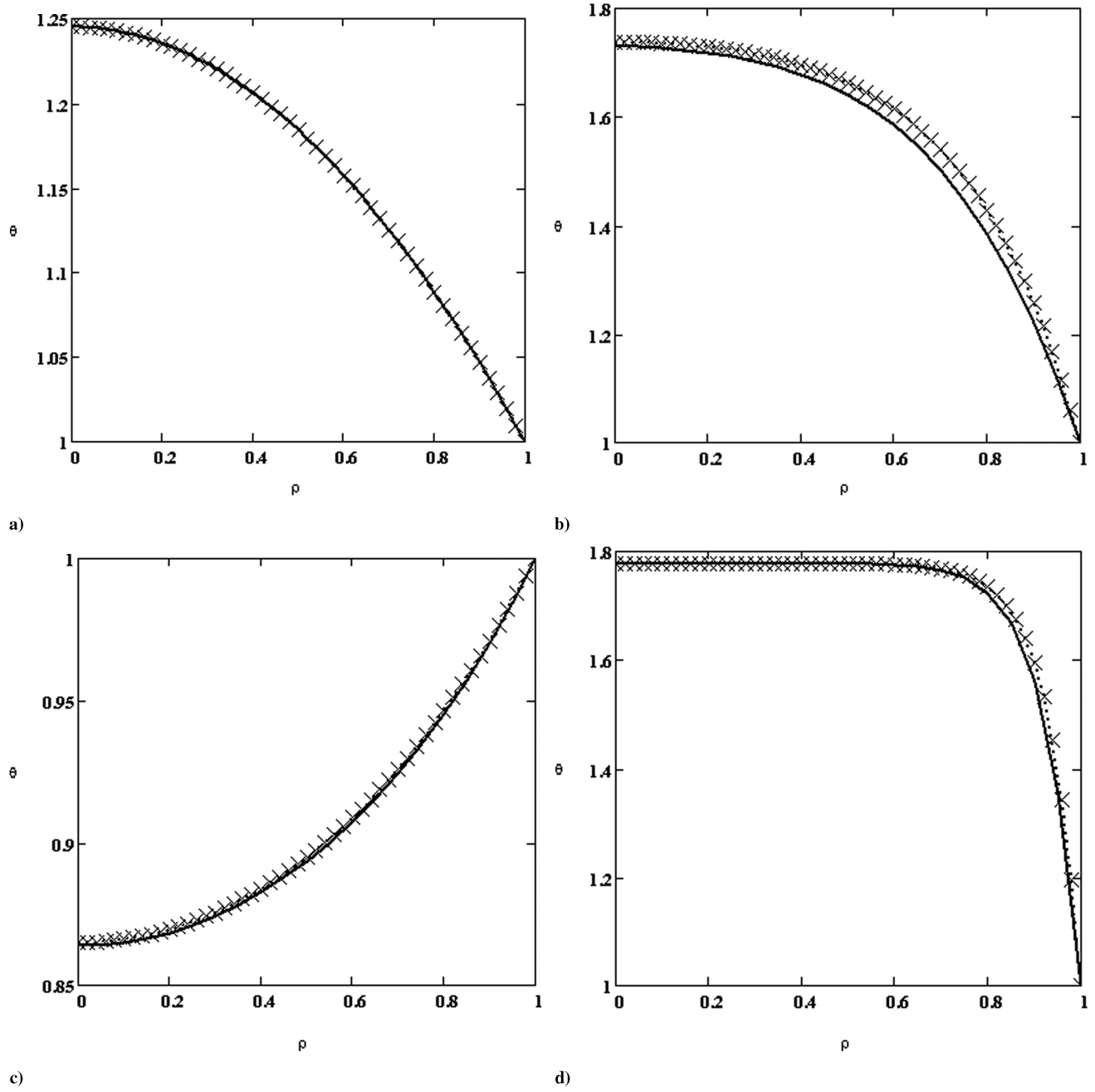

Fig. 6 Dimensionless temperature profiles from the linear solution, Eq. (13), and comparison with Runge–Kutta integration for a) $A = 0.01$ and $B = 100$, b) $A = 1$ and $B = 10$, c) $A = 1$ and $B = 0.1$, and d) $A = 10$ and $B = 10$ (solid curve: Eq. (13); X-X-X: R-K integration).

the dimensionless temperature profiles of the R-K and the linear solution occurs at $\rho = 0.9$.

E. Accuracy of the Linear Solution

The accuracy of using Eq. (12) for determining B from the measured $\Delta\theta$ was assessed by calculating the corresponding value of B used in the Runge–Kutta calculation. That is, B_L was calculated using Eq. (12) for the values of A and the corresponding value of θ_o calculated using R-K that are listed in Table 1. The error was then calculated assuming the values of B used in R-K as the exact values. This was done for values of $A = 0.001, 0.01, 0.1, 1.0$, and 10 and for $B = 5$, 20, 50, and 500 in addition to those listed in Table 1. The computed error in B_L is plotted in Fig. 7 as function of $\Delta\theta$ and for the previously stated values of A. A maximum error of about 6% is noted. The maximum error occurs when the value of θ_o falls in the rapid rise region of the curves shown in Fig. 3. Considering the accuracy of temperature measurements with precision thermocouples to within a tolerance of 0.5 K, the use of Eq. (12) for calculating B from the measured value of $\Delta\theta$ is practical and justified when the accuracy in the heat flux measurement is needed to within $\pm 10\%$.

The dimensionless irradiation parameter B, obtained from Eq. (12), was also compared with the corresponding values computed using the curve fits [Eq. (24) of [1]]. The comparison is presented here for $A = 0.787$ shown in the third column of Table 2 of [1]. These cases are in the midrange of A and are listed with relatively small errors between the curve fits and the exact values obtained using a Green's function approach. As shown in Fig. 8, Eq. (12) yielded a maximum error in B of 2.32%, which is about half of the maximum error of the curve fits of [1]. Moreover, the errors in B calculated using the curve fits increase beyond $B = 69.1$, whereas the errors become less than 0.15% when B is calculated using Eq. (12). A similar computation of the errors was made for the cases shown in the sixth row ($B = 69.1$) in Table 2 of [1]. The cases listed in the sixth row ($B = 69.1$) of Table 2 of [1] were for nominally the same value of $\Delta\theta \approx 1.88$. The good accuracy of Eq. (12) for

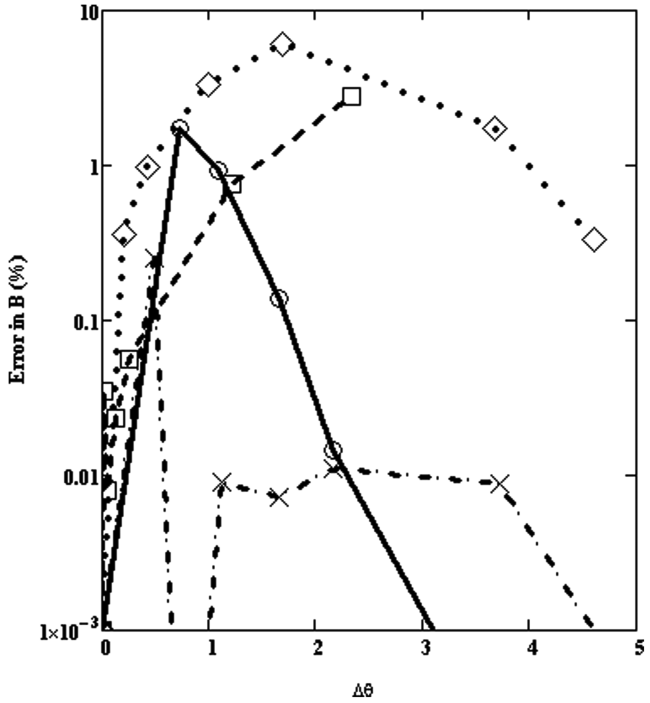

Fig. 7 Error in the measured irradiation parameter B calculated from the linear solution, Eq. (12), assuming B computed using Runge–Kutta numerical integration as the exact value (diamonds-dots: $A = 0.10$; squares-dashes: $A = 0.01$; circles-solid lines: $A = 1.0$; and X-dash-dot lines: $A = 10$).

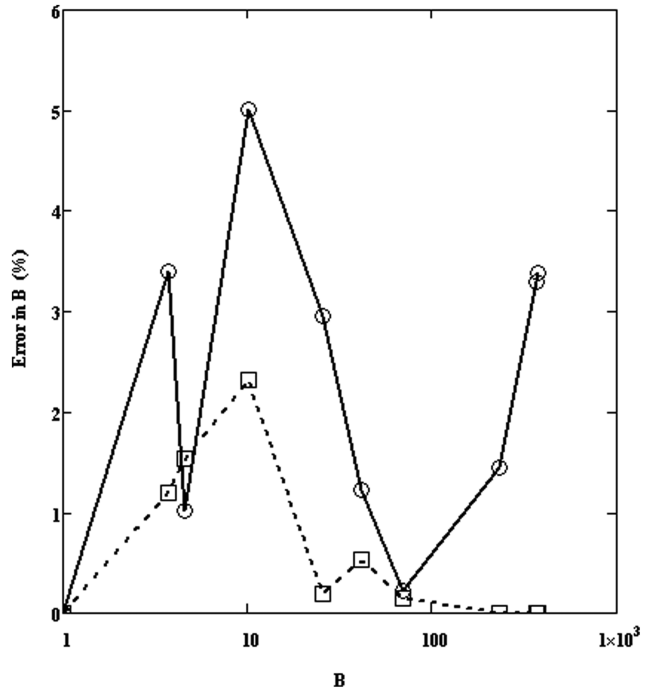

Fig. 8 Percent error using the linear solution to compute B, Eq. (12) compared with curve fits of [1], and Eq. 24 of [1] for $A = 0.787$ (squares-dashed lines: Eq. (12) and circles-solid lines: curve fits, Eq. (24) of [1]).

calculating the irradiation parameter B is due to the proper accounting of the heat radiated from the foil close to its center by means of the linear representation of the quartic, Eq. (14), in which the temperature is high relative to that at the edge.

F. Heat Flux Gauge Calibration and Size Considerations

All instruments are prone to inherent errors. For thin-foil heat flux gauges, errors are due to the following:

1) The copper lead wire at the center conducts heat away from the foil at its center.

2) Large temperature excursions affect the effective thermal conductivity and give rise to electromotive forces that increase the effective thermal conductivity of the foil due to the motion of the electrons [11].

3) There is contact resistance at the edge of the foil on which it is mounted on the copper heat sink.

4) There is a difference in temperature of the copper heat sink from the temperature of the irradiated surface (wall) of the test article especially when B is large.

5) The foil surface preparation can affect the emissivity of the foil. In the preceding analysis, the thermal conductivity was assumed to be constant.

For a value of θ_o of 2, the center temperature is 600 K when the copper heat sink is at 300 K. Therefore, an effective value of the gauge parameter A is appropriate to account for the temperature dependence of the thermal conductivity and other physical parameters of the foil. Values of $\Delta\theta$ greater than 2 are encountered under high-irradiation fluxes with corresponding foil temperatures greater than 400°C. A copper-constantan thermocouple, type T, is rated for use up to 350°C [12]. Therefore, such a gauge is useful for B less than about 81 when T_R is 300 K. Also, high temperatures can cause thermal stresses in the constantan foil, thereby compromising the structural integrity of the gauge.

To account for inherent errors, a calibration of each gauge is usually performed. Here, it is suggested to introduce an empirically determined factor multiplying the argument of the modified Bessel function in Eq. (12) (i.e., $4A\theta_o^{3/4}$) to suitably fit the calibration data.

For an optimized gauge design, it is desirable to have the gauge temperature close to the surface temperature of the test article. The solution of Eq. (1) indicates that an isothermal gauge with $\theta = 1$ is obtained when either $A = 0$ or $B = 1$. The former can be satisfied when the thermal conductivity of the foil is very large, whereas $B = 1$ is satisfied by adjusting the sink temperature according to $T_R = (B/\sigma)^{1/4}$. This might require a cooling fluid. Physically, $B = 1$ implies that the exact same amount of heat irradiated *onto* the gauge would have to be radiated away from the gauge regardless of the value of the gauge parameter, because in this case, there is no heat transfer by conduction, as $dT/dr = 0$. To avoid disturbing the temperature field by the presence of the gauge, it is best to have the copper-heat-sink temperature close to that of the surface of the test article as suggested in [1]. The results presented here indicate that the dimensionless gauge parameter should be greater than 0.1, in accord with [1], by selecting the geometric parameters of the gauge (i.e., the foil thickness) and radius R as well as the surface emissivity. This will reduce the sensitivity of the gauge and will avoid signal noise problems. However, to avoid the plateau region evident in Fig. 3, the maximum value of the gauge parameter should be selected according to the expected value of B to have $AB^{3/4}$ less than about 10. Finally, consistent with standard calibration practices [4,5], it is recommended here that the calibration data be fitted using an expression similar to Eq. (12) with a suitably adjusted empirical factor in the argument of Io.

III. Conclusions

A six-term series solution of the nonlinear heat equation for a circular-foil heat flux gauge that is exposed to a blackbody heat source in a vacuum environment has been presented. Numerical experimentation shows that the truncated series solution yields accurate values of θ for $A \leq 1$ and $B \leq 100$. A linear solution, which was extracted from the series solution, yields a simple-yet-accurate formula for determining the theoretical dimensionless irradiation parameter for all values of the dimensionless gauge parameter. The formula is exact when $A = 0$, A is infinite, and $B = 1$. To fit the calibration data, it is suggested to introduce a correction factor in the argument of the modified Bessel function that appears in the nonlinear formula for B_L, Eq. (12). The linear solution offers physical insight and can be used to simplify the optimization and calibration of the gauge. Finally, the solution presented here is useful

for designing and calibrating thin-foil heat flux gauges with semiconductor materials other than constantan, such as a type-S T/C: platinum–10% rhodium–platinum, which is suitable for operation at temperatures up to 1750°C and hence for measuring the irradiation H, corresponding to dimensionless irradiation parameters B in the hundreds to thousands.

References

[1] Liechty, B. C., Clark, M. M., and Jones, M. R., "Nonlinear Thermal Model of Circular Foil Heat Flux Gauges," *Journal of Thermophysics and Heat Transfer*, Vol. 21, No. 3, July–Sept. 2007, pp. 468–474. doi:10.2514/1.24471

[2] Hornbaker, D. R., and Rall, D. L., "Heat Flux Measurements: "A Practical Guide"," *Instrumentation Technology*, Vol. 51, Feb. 1968, pp. 51–56.

[3] Lee, Y. H., Koo, S. W., and Choi, J. H., "Heat-Flux Gage, Manufacturing Method and Manufacturing Device Thereof," Agency for Defence Development, Daejeon, Korea, U.S. Patent No. 6,837,614 B2, 4 Jan. 2005.

[4] Anon., "Standard Test Method for Measuring Heat Flux Using a Copper-Constantan Circular Foil, Heat-Flux Gage," *ASTM Book of Standards*, Vol. 15.03, Standard E511-73(1994)e1, American Society for Testing and Materials, West Conshohocken, PA, Nov. 2000.

[5] Murthy, A. V., Fraser, G. T., and De Witt, D. P., "A Summary of Heat Flux Sensor Calibration Data," *Journal of Research of the National Institute of Standards and Technology*, Vol. 110, No. 2, Mar.–Apr. 2005, pp. 97–100.

[6] Beckwith, T. G., Buck, L. N., and Marangoni, R. D., *Mechanical Measurements*, 3rd ed., Addison Wesley Longman, Reading, MA, 1982, pp. 571–574.

[7] Doebelin, E. O., *Measurement Systems Application and Design*, McGraw–Hill, New York, 1997, pp. 576–581.

[8] Fausett, L., *Numerical Methods Using MathCAD*, Prentice–Hall, Upper Saddle River, NJ, 2002, pp. 585–605.

[9] Shieh, T.-M., *Numerical Heat Transfer*, Hemisphere, Washington, D.C., 1984, pp. 114–121.

[10] Abramowitz, M., and Steven, I. A., *Handbook of Mathematical Functions with Formulas, Graphs, and Mathematical Tables*, Dover, New York, 1965, pp. 375.

[11] Angrist, S. W., *Direct Energy Conversion*, 4th ed., Allyn Bacon, Boston, 1982, p. 106.

[12] Anon., *Temperature Handbook*, Vol. 28, Omega Engineering, Stamford, CT, pp. H-3, Z-18.